On the observed connection between Arctic sea ice and Eurasian snow in relation to the winter North Atlantic Oscillation

María Santolaria-Otín, Javier García-Serrano, Martin Ménégoz, Joan Bech

ENVIRONMENTAL RESEARCH
LETTERS

On the observed connection between Arctic sea ice and Eurasian snow in relation to the winter North Atlantic Oscillation

To cite this article before publication: María Santolaria-Otín *et al* 2020 *Environ. Res. Lett.* in press https://doi.org/10.1088/1748-9326/abad57

On the observed connection between Arctic sea ice and Eurasian snow in relation to the winter North Atlantic Oscillation

María Santolaria-Otín[1,2] & Javier García-Serrano[1,3] & Martin Ménégoz[1,2] & and Joan Bech[3]

[1]Barcelona Supercomputing Center (BSC), Barcelona, Spain

[2]Institut des Géosciences de l'Environnement (IGE), Université Grenoble Alpes, France

[3]Group of Meteorology, Universitat de Barcelona (UB), Spain.

E-mail: santolariaotin.maria@gmail.com

December 2019

Abstract. Sea ice concentration (SIC) in the eastern Arctic and snow cover extent (SCE) over central Eurasia in late autumn have been proposed as potential predictors of the winter North Atlantic Oscillation (NAO). Here, maximum covariance analysis is used to further investigate the links between autumn SIC in the Barents-Kara Seas (BK) and SCE over Eurasia (EUR) with winter sea level pressure (SLP) in the North Atlantic-European region over 1979-2019. As shown by previous studies, the most significant covariability mode of SIC/BK is found for November. Similarly, the covariability with SCE/EUR is only statistically significant for November, not for October. Changes in temperature, specific humidity, SIC/BK and SCE/EUR in November are associated with a circulation anomaly over the Ural-Siberian region that appears as a precursor of the winter NAO; where the advection of climatological temperature/humidity by the anomalous flow is related to SCE/EUR and SIC/BK anomalies.

Keywords: North Atlantic Oscillation, Teleconnection, Sea Ice, Snow Cover

1. Introduction

The North Atlantic Oscillation (NAO) is the most prominent pattern of atmospheric circulation variability in the Euro-Atlantic sector and has a strong influence on the regional surface climate (e.g., **?**, **?**). Understanding the processes that potentially drive the NAO state is crucial to improve its predictability. Many recent studies have stressed the potential predicting role of eastern Arctic sea ice and continental snow over Eurasia in autumn, with a reduction of sea ice concentration (SIC) in the Barents-Kara Seas and an increase of snow cover extent (SCE) across Siberia that would favor a negative NAO phase during the subsequent winter (e.g., **?**, **?**, **?**, **?**, **?**).

Sea ice reduction acts as a source of heat and moisture fluxes that can impact both local and large-scale atmospheric circulation. Observational studies (e.g., **?**, **?**) and numerical simulations with both atmospheric general circulation models (AGCMs) (e.g., **?**, **?**, **?**, **?**) and coupled climate models (e.g., **?**, **?**) have found that an anomalous anticyclone over northern Eurasia related to low SIC/BK in late-autumn tends to evolve into a negative NAO-like pattern in winter through a lagged stratospheric pathway. The tropospheric anomalies related to low SIC/BK display a Rossby wave-like anomaly crossing Eurasia, reinforcing the climatological wave pattern. An upward propagation of wave activity finally reaches the stratosphere and weakens the polar vortex. The downward response decelerates the westerlies in the North Atlantic sector shifting the storm-tracks southward, which is tied to a negative NAO phase (e.g., **?**, **?**). Yet, causality in this chain of processes has to be confirmed (**?**, **?**, **?**).

Snow cover variations affect the atmosphere via changes in reflected shortwave solar radiation (albedo), emissivity of longwave radiation, insulation of the atmosphere from

the soil layers below, and latent-heat and water release in association with melting (e.g., **?**). Observational studies (e.g., **?**) and GCM experiments (e.g., **?**, **?**, **?**, **?**, **?**, **?**, **?**) showed that an increase in the continental SCE over Eurasia (SCE/EUR) in late autumn can also favor a negative NAO phase in winter via troposphere-stratosphere-troposphere interactions. The mechanism relies on the regional radiative cooling induced by positive SCE anomalies over central Eurasia, which modifies the structure and vertical propagation of planetary-scale wave activity eventually triggering a similar stratospheric pathway as described above. But again, as for SIC/BK, causality related to SCE/EUR has yet to be fully established (**?**, **?**).

The stationarity of the SIC-NAO and SCE-NAO relationships has been questioned (e.g., **?**, **?**) due to the shortness of the observational record and the modulation of the polar vortex by the Quasi-Biennal Oscillation (**?**, **?**). Besides, the connection between these two potential predictors of the winter NAO, i.e. SIC/BK and SCE/EUR, is still an open question (**?**). Although previous observational and modeling studies have shown that sea-ice reduction over the eastern Arctic is associated with increased snowfall over Siberia (e.g., **?**, **?**, **?**, **?**, **?**, **?**, **?**, **?**), the physical processes underlying this relationship are unclear. There is also a lack of consensus to determine both the respective contributions of sea-ice and snow-cover anomalies to the winter NAO predictability and the exact timing of their lagged influence on the atmospheric circulation (e.g., **?**).

The aim of this study is to comprehensively set the observed statistical relationship between SIC/BK and SCE/EUR with the winter NAO and discuss the associated atmospheric circulation, in order to assist model validation in targeted sensitivity experiments to come (**?**, **?**). The novelty relies on getting insight into the dynamics underlying the SIC/BK and SCE/EUR anomalies linked to the atmospheric precursor of the winter NAO, namely the Ural-Siberian pattern.

2. Data and Methodology

In this study, empirical orthogonal function (EOF; **?**) and maximum covariance analysis (MCA; **?**) are used to describe the spatio-temporal structure of SIC/BK and SCE/EUR variability as well as their covariability with winter SLP anomalies over the period 1979-2019. EOF analysis has been employed to test the robustness of the MCA results. The NAO index is defined as the leading principal component (PC), namely standardized time series, corresponding to the leading mode (first EOF) of sea level pressure anomalies in the North-Atlantic-European region (Figure 1a)(NAE: $20^{o}\mathrm{N} - 90^{o}\mathrm{N}, 90^{o}\mathrm{W} - 40^{o}\mathrm{E}$; e.g. **?**).

MCA is a singular value decomposition (SVD) applied to the covariance matrix of two fields that share a common sampling dimension (the actual time) but can be spatially independent. The output consists of pairs of spatial patterns, each one corresponding to a field, and associated standardized time-series called expansion coefficients (ECs). Each MCA mode is characterized by the squared covariance (sc) which is the eigenvalue of the covariance matrix, the squared covariance fraction (scf) which is a measure of the fraction of explained covariance compared to other modes, and the correlation between the expansion coefficients (cor).

MCA is respectively applied to SIC in the Barents-Kara Seas (BK: $50^{o}\mathrm{N} - 90^{o}\mathrm{N}, 30^{o}\mathrm{W} - 120^{o}\mathrm{E}$), and Eurasian SCE (EUR: $20^{o}\mathrm{N} - 90^{o}\mathrm{N}, 0^{o} - 150^{o}\mathrm{E}$) for autumn (from September to November) as predictor fields and winter SLP/NAE as predictand field (seasonal average for DJF). The first MCA mode is analyzed in both cases. A Monte Carlo test based on 100 permutations shuffling only the atmospheric field (i.e. SLP) with replacement is performed to determine the statistical significance of these MCA modes. By performing MCA upon each resampling we generate a probability density function (PDF) that is used to compute the significance level (hereafter simply p-value) which corresponds to

the number of randomized values (sc, scf or cor) that exceed the actual value being tested (e.g., **?**).

Monthly SIC data are provided by HadISST (Hadley Center Sea Ice and Sea Surface Temperature; **?**) at $1.0^o \times 1.0^o$ resolution and SCE data from the Global Snow Laboratory at Rutgers University (**?**). For SCE, October is defined as the average of the calendar weeks 40-44 (**?**), and November of the weeks 44-48. Compared to **?** for SCE and **?** for SIC, our choice of dataset does not affect results. Monthly data of atmospheric variables are given by ERA-Interim reanalysis available from the European Center for Medium-Range Weather Forecasts (ECMWF) at $2.5^o \times 2.5^o$ resolution (**?**). Forecast-accumulated turbulent (sensible plus latent) and radiative (shortwave plus longwave) heat fluxes initialized twice a day (00, 12h) from ERA-Interim are also used; upward is positive, from surface to atmosphere. All anomalies are detrended before analysis to focus on the interannual variability, aiming to exclude any long-term relationship among variables. Different detrending methods (1st-, 2nd- and 3th-order polynomial fits) have been evaluated to assess robustness of the results; in the manuscript we only show cubicly detrended anomalies because of the strong non-linear trends in SIC/BK, but the results are largely insensitive to the detrending method.

To explore the dynamics involved in the statistical relationships, regression maps are computed by projecting different anomalous fields onto a time-series, either the NAO index or the MCA expansion coefficients. In this case, the statistical significance of the regressed anomalies is evaluated with a two-tailed Students t-test at 95% confidence level.

3. Results

3.1. Covariability: SIC/BK and SCE/EUR

The leading MCA mode based on September SIC/BK anomalies explains 58% of scf (p-value 29%), with a sc of 1.35×10^7 (p-value 16%) and yields a cor of 0.56 (p-value 27%)(Table 1). These high p-values indicate a low confidence level for this relationship, associated with a low signal-to-noise ratio and non-significant predictability (e.g., **?**, **?**). For October, the leading MCA mode explains 85% of scf (p-value 1%), with a sc of 5.09×10^7 (p-value 0%),and yields a cor of 0.60 (p-value 3%)(Table 1). The leading MCA mode based on November SIC/BK anomalies explains 82% of scf (p-value 2%), with a sc of 3.35×10^7 (p-value 0%) and yields a cor of 0.63 (p-value 1%)(Table 1). The MCA-SIC/BK in October is also significant, but there is no clear atmospheric mechanism responsible for a lagged relationship with the winter NAO (see **?**). According to **?**, the potential influence of October SIC/BK anomalies on the winter Euro-Atlantic climate would rely on its contribution to November SIC/BK anomalies. On the other hand, the dynamics associated with SIC/BK anomalies in November are much more plausible and largely reported. It could involve a stratospheric pathway (e.g., **?**, **?**, **?**) and represent a suitable predictability source of the winter Euro-Atlantic climate (e.g., **?**, **?**, **?**, **?**). Thereby, the analysis is focused hereafter on November SIC/BK variability. To simplify the nomenclature, we will refer to the MCA covariability mode between SIC/BK in November and SLP/NAE in winter as MCA/SIC_N.

Figure 1b shows the regression map of SIC anomalies in November onto the SIC expansion coefficient of MCA/SIC_N. The resulting SIC pattern shows negative anomalies (i.e. sea-ice reduction) over the northern Barents Sea and the whole Kara Sea. The SLP covariability pattern of MCA/SIC_N (not shown) strongly resembles the negative phase of the NAO (Figure 1a). The SLP expansion coefficient of MCA/SIC_N

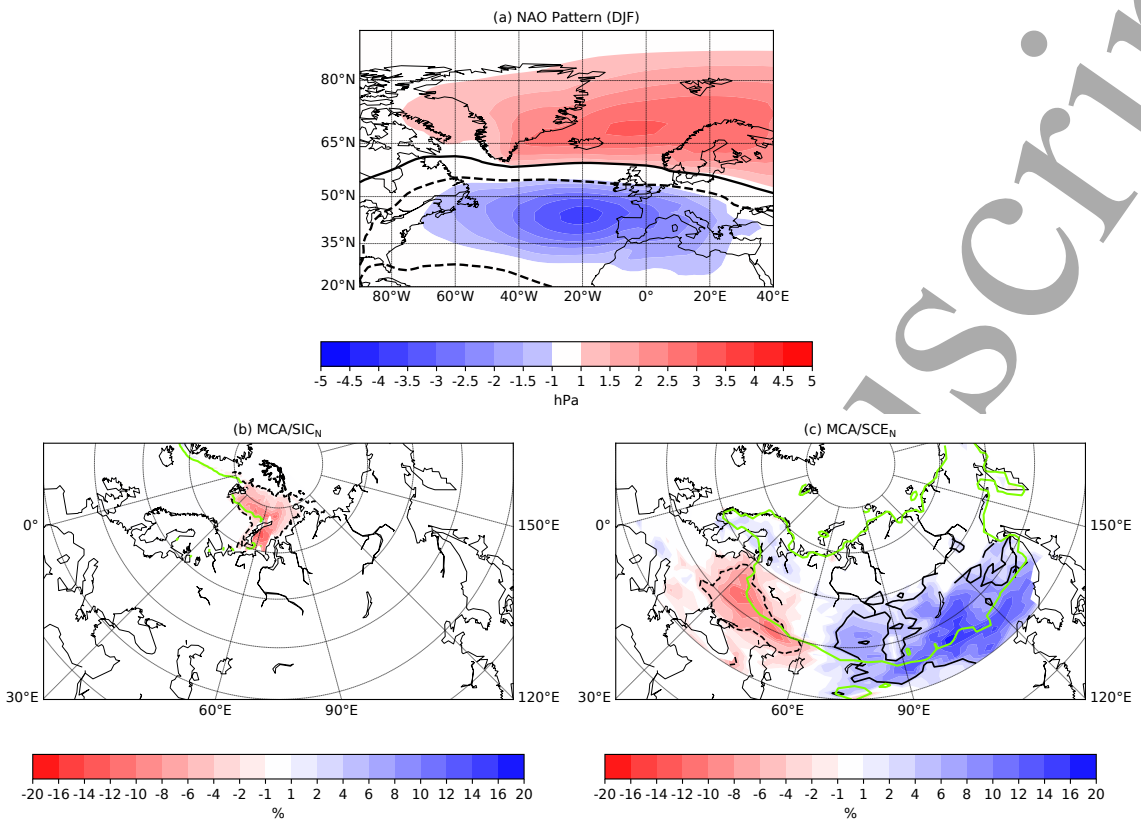

Figure 1. (a) Leading EOF of detrended sea level pressure anomalies (hPa) in winter (DJF) over the North Atlantic-European (NAE) region, with a fraction of explained variance of 47.9 % ; note that the negative phase of the NAO is shown. Leading MCA mode between (b) SIC over Barents-Kara Seas (%) and (c) SCE over Eurasia (%) in November with winter (DJF) SLP over the North Atlantic-European region (hPa). Statistically significant areas at 95 % confidence level based on a two-tailed Student's test are contoured. Green contours stand for the climatological sea-ice edge estimated at 15% in (b) and the climatological snow cover edge estimated at 50% in (c); the full field of SIC and SCE climatology can be found in Figure S1.

has indeed a correlation of -0.99 with the winter NAO index, illustrating that the NAO has been effectively captured as predictand.

Caution is required to assert cause and effect based on observational data and MCA results. Concerning the former, several studies using AGCM simulations (e.g., **?**, **?**, **?**) have also found a lagged teleconnection between SIC/BK anomalies and the NAO, although the timing may be model dependent (**?**). As for the latter, we further explore the suitability of SIC/BK as predictor. The SIC expansion coefficient of MCA/SIC$_N$ is compared with the leading principal component (PC1) of SIC over the eastern Arctic

and over the Northern Hemisphere in November: the SIC expansion coefficient yields a high correlation with both the regional PC1 (0.98) and the hemispheric PC1 (0.93). Likewise, the lagged regressions of winter SLP onto the two PC1s are almost identical to that of the SIC expansion coefficient (not shown), which is consistent with alternative approaches based on area-averaged SIC indices (**?**, **?**). Hence, the covariability mode of MCA/SIC_N is associated with a leading mode of SIC variability *per se*. Note that the SIC pattern of MCA/SIC_N corresponds to the second EOF of turbulent heat flux in **?**, with a strong ocean-to-atmosphere forcing (see also **?** and **?**); which is unrelated to the so-called "Warm Arctic-Cold Siberia" (WACS) pattern in winter. It follows that November SIC/BK anomalies can be considered as a potential predictor of the subsequent winter NAO. Lagged regression of SIC anomalies in November onto the winter NAO index (Figure S2a) support this conclusion.

Analogous to the procedure followed for SIC/BK, MCA based on SCE/EUR anomalies in late autumn (October, November) have been performed. Note that September has not been considered because there is almost no snow cover over the continent at that time of the year (e.g., **?**). The leading MCA mode for October SCE/EUR anomalies explains 52% of scf (p-value 45%), with a sc of 1.90×10^7(p-value 26%), and yields a cor of 0.69 (p-value 33%). For November, the leading MCA explains 74% of scf (p-value 0%), with a sc of 4.89×10^7(p-value 0%) and yields a cor of 0.76 (p-value 13%). Extending the period using reanalyzed SCE data (instead of satellite-derived products) would probably not lead to better statistical results (**?**) especially when considering the potential non-stationarity of the snow-NAO relationship (**?**). In contrast to previous studies that suggested a statistically significant relationship between October SCE/EUR and the winter NAO (e.g., **?**, **?**, **?**), these results reveal that the covariability of October SCE/EUR with winter SLP/NAE is largely statistically

non-significant, namely not discernable from noise. However, we found that November SCE/EUR anomalies tend to be followed by NAO-like atmospheric variability, a result consistent with the monthly analysis of **?**.

This finding is supported by the lagged regression maps of autumn SCE/EUR anomalies onto the winter NAO index, where October does not show statistically significant anomalies over Eurasia (not shown) but November does so (Figure S2b). Thus, in the following the analysis is restricted to November SCE/EUR. As for SIC, we will refer to the leading MCA covariability mode between SCE/EUR in November and SLP/NAE in winter as MCA/SCE_N for the sake of readability. Figure 1c shows the covariability mode of SCE from MCA/SCE_N, exhibiting statistically significant positive anomalies (i.e. snow cover increase) over central-eastern Eurasia. The SLP covariability of MCA/SCE_N displays a negative NAO-like pattern (not shown, but similar to Figure 1a) and its expansion coefficient correlates at -0.99 with the winter NAO index.

The SCE expansion coefficient of MCA/SCE_N attains only a correlation of 0.58 (0.30) with the first (second) EOF of November SCE/EUR. The fraction of explained variance of the two leading EOFs is very low (EOF1=15%, EOF2=12%), indicating that they are not well separated statistically (following **?**) and illustrating that SCE is a noisy field. This result implies, as opposed to the case of November SIC/BK, that the covariability of MCA/SCE_N does not rely on a dominant variability mode of snow cover itself, which questions the feasibility of using SCE/EUR as a potential predictor for the NAO.

Repeating the analysis with snow depth (SD) from ERA-Interim yields consistent results: namely, the MCA with October SD not being significant and the one with November SD showing hints of significance. In the latter case, as opposed to using satellite-derived SCE, sc and scf are higher but above 10% significance level, while the

	September	**October**	**November**
(**MCA/SIC$_N$**)			
scf (p-value)	58 % (29%)	85 % (1%)	82% (2%)
sc (p-value)	1.35×10^7(16 %)	5.09×10^7(0%)	3.53×10^7 (0%)
cor (p-value)	0.56 (27 %)	0.60 (3%)	0.63 (2%)
(**MCA/SCE$_N$**)			
scf (p-value)	/	52 % (45%)	74 % (0%)
sc (p-value)	/	1.90×10^7(26%)	4.89×10^7 (0%)
cor (p-value)	/	0.69 (33%)	0.76 (13%)

Table 1. Results of the MCA covariability analysis between autumn SIC/BK and SCE/EUR with winter SLP/NAE for the period 1979-2019. The squared covariance fraction (scf), the squared covariance (sc) and the correlation between the expansion coefficients (cor) are listed for each mode, together with the significance level (p-value).

correlation between expansion coefficients is smaller but significant at 3% (cor=0.52). The MCA/SD$_N$ pattern (not shown) and the regression of November SD/EUR anomalies onto the winter NAO index (Figure S3) display positive anomalies over central Eurasia, particularly west of the Baikal Lake.

3.2. Ural-Siberian anticyclone (SCAND)

To shed light on the large-scale atmospheric circulation in November preceding the winter NAO, the climatology and variability of SLP over Eurasia is analysed. This is compared to contemporaneous SLP anomalies associated with MCA/SIC$_N$ and MCA/SCE$_N$, together with the SLP precursor of the NAO obtained by regressing November SLP anomalies onto the winter NAO index.

Figure 2b shows the regression map of Northern Hemisphere (NH) SLP anomalies onto the first EOF of November SLP anomalies over Eurasia ($20^oN - 90^oN, 0^o - 150^oE$; EOF1). This regional EOF1 strongly resembles the hemispheric EOF1 (not shown; r=0.89), which is also a dominant mode of variability later in the season - in winter (**?**). The pattern is dominated by an anticyclonic circulation anomaly over the subarctic Eurasian region, but exhibits a dipole-like structure with a weaker center of opposite sign

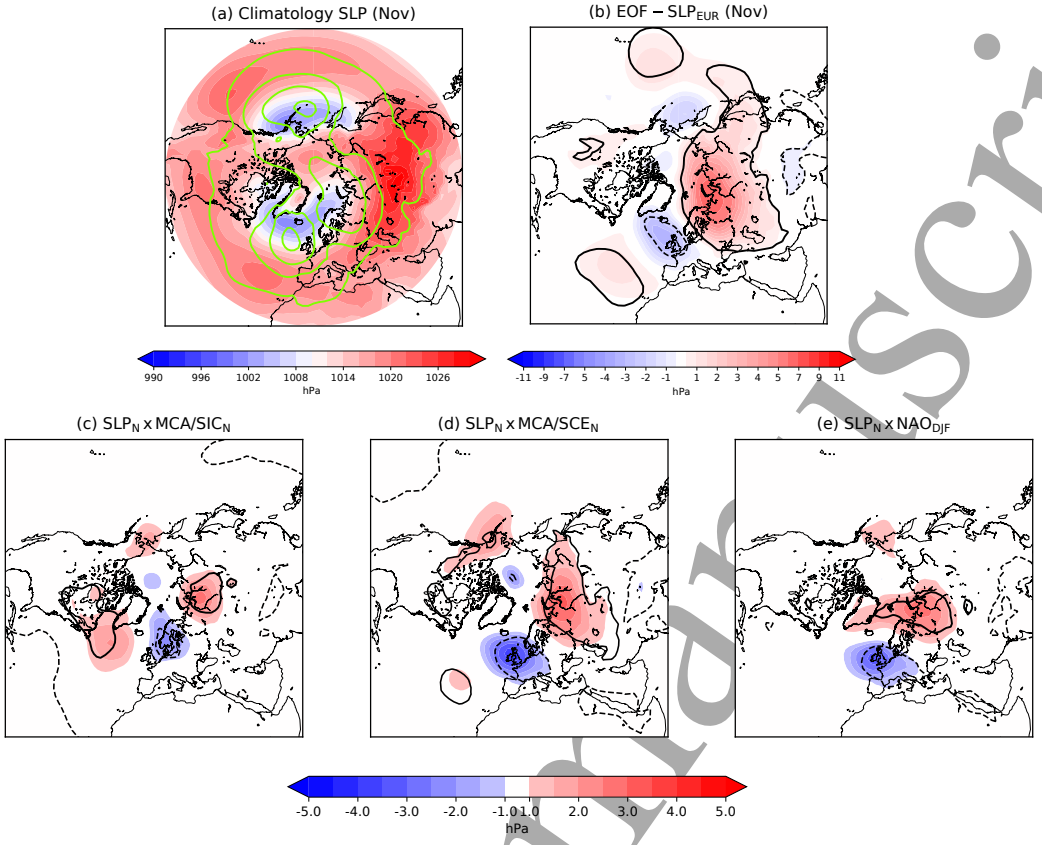

Figure 2. (a) Climatology (hPa ; shading) and standard deviation (ci=2hPa ; green contours) of SLP in November. Regression map of detrended Northern Hemisphere sea level pressure anomalies (hPa) in November onto (b) the leading PC from the EOF analysis of November SLP over Eurasia (40°N -90°N , 0°-150°E ; 41.5 % fraction of explained variance), (c) the MCA/SIC$_N$ expansion coefficient, (d) the MCA/SCE$_N$ expansion coefficient and (e) the winter NAO index - multiplied by -1. Statistically significant areas at 95 % confidence level based on a two-tailed Student's test are contoured.

over western Europe. The identification of this surface anticyclone has been ambiguous in the literature. It appears to be related to Ural blocking at daily time-scales (e.g., **?**, **?**), but it also constitutes a prominent mode of variability at monthly and seasonal time-scales (e.g., **?**, **?**). **?** tentatively named it as the Russian (RU) pattern, but here it will be referred to as the Ural-Siberian (U-S) pattern. Interestingly, the centers of action of EOF1 (Figure 2b) tightly project on the areas of maximum interannual variability (i.e. standard deviation; green contours in Figure 2a), as it is also the case for the mid- (500hPa; **?**) and upper-tropospheric (200hPa; **?**) geopotential height. The leading

mode of Eurasian geopotential height variability in the mid-upper troposphere, which has a better-defined wave-like signature (Figure S4a at 300hPa; e.g., **?**), can be more easily identified as the Scandinavian (SCAND) pattern, a mode of internal variability associated with Rossby wave propagation dynamics and maintained by transient-eddy feedback (e.g., **?**, **?**). Note that the U-S pattern of SLP corresponds to the surface projection of the SCAND pattern at upper levels, and the other way around, since they show a marked barotropic structure (e.g., **?**, **?**).

The statistically significant SLP anomalies preceding the winter NAO also show a dipole-like structure (Figure 2e), projecting on the centers of the U-S pattern over the Siberian coast and the British Isles (Figure 2b). At 300hPa, the winter NAO is preceded by a wave-like structure over Eurasia, which also projects on the SCAND pattern at upper levels (Figure S4c). These results are consistent with **?**, **?**, **?** and **?** who showed that the winter NAO tends to be preceded by a wave-like anomaly over Eurasia, which triggers a stratospheric pathway. These findings suggest that the U-S/SCAND pattern in November may eventually evolve into the winter NAO with a 1-month lead time and might be considered a precursor of the winter NAO. This line of reasoning has been recently confirmed by **?**.

Figure 2c and 2d show the regression map of contemporaneous SLP anomalies onto expansion coefficients of SIC and SCE from MCA/SIC_N and MCA/SCE_N, respectively. The anomalous dipole-like pattern associated with MCA/SCE_N(Figure 2d) has a strong resemblance to EOF1 (Figure 2b), which is consistent with previous studies using other autumnal Eurasian SCE indices (e.g., **?**, **?**). It is worth noting that there is no signal over the Siberian High region (reddest areas at mid-latitudes of Figure 2a), which would be expected from the radiative feedback linked to Eurasian snow cover anomalies (Figure 1c and S2b). However, the anomalous Ural-Siberian anticyclone in Figure 2b has been

usually interpreted as a north-westward expansion of the Siberian High in response to increased SCE over central Eurasia (**?**, **?**, **?**, **?**, **?**), although the U-S pattern develops over the subpolar low-pressure belt along the Siberian coast (blue shading in Figure 2a), linked to local transient-eddy activity (e.g., **?**) and cyclone tracks (e.g., **?**). In fact, no AGCM study prescribing positive Eurasian SCE anomalies has reported such a circulation response. Instead, they have found a regional baroclinic structure associated with a reinforced Siberian High at surface and cyclonic circulation anomalies in the upper troposphere (**?**, **?**, **?**, **?**, **?**, **?**, **?**, **?**); the most significant being the reinforcement of the Siberian High (**?**, **?**). Thus, there is no modelling evidence supporting the impact or triggering role of SCE/EUR anomalies on the U-S/SCAND pattern. This line of reasoning suggests that the SCE/EUR anomalies in November related to the winter NAO (Figure 1c and S2b) might be potentially driven by the Ural-Siberian anticyclone (Figure 2b) rather than the other way around, which is in agreement with **?** and **?** and further discussed in Section 3.4.

On the other hand, the dipole-like pattern of SLP anomalies associated with MCA/SIC_N (Figure 2c) is slightly different from the other patterns, as the centers of action are located downstream, with the anticyclonic anomalies shifted toward the continent and the cyclonic anomalies displaced toward the Nordic Seas. The vertical structure of the anticyclonic anomalies over the Siberian coast reveals some baroclinicity(cf. Figure S4a), in agreement with AGCM simulations (e.g., **?**), which suggests a possible contribution of SIC/BK variability on the U-S pattern (**?**) that is further discussed in section 3.4.

3.3. Linkage between SIC/BK and SCE/EUR

To explore the relationship between November SIC/BK and SCE/EUR in relation to the winter NAO, regional near-surface conditions of temperature (T925), specific humidity

(q925) and horizontal wind are analyzed at 925hPa (Figure 3). As our framework does not allow disentangling cause and effect, the analysis below is focused on lagged regressions in November onto the winter NAO index, thereby assessing the observed NAO precursors in an objective way. Regressions onto the expansion coefficients of MCA/SCE_N or MCA/SIC_N yield very similar results.

Climatology in this region shows a cold and dry environment east of Scandinavia (eastern Arctic/eastern Siberia), whereas in western Europe warm and wet conditions prevail (Figure 3a,b). Figure 3c and 3d show regression maps of November T925 and q925 onto the winter NAO index, respectively. Warm and wet anomalies are found over the Barents-Kara Seas in relation to sea-ice reduction (c.f. Figures 1b,S2a) while cold and dry anomalies extend across Eurasia in association with the increase in snow cover (c.f. Figures 1c,S2b), although only the latter is statistically significant. SIC/BK reduction and SCE/EUR increase are source and sink of humidity, respectively, as discussed in previous observational and modelling studies (e.g., **?**, **?**, **?**). Noteworthy, it is usually assumed that the connection between SIC/BK and SCE/EUR is as follows: sea-ice reduction providing extra evaporation, increased moisture flux inland, and enhanced snowfall over Eurasia (e.g., **?**, **?**). However, model results show that the direct impact of sea-ice reduction on snowfall would mainly apply to the Siberian coast (e.g., **?**, **?**, **?**). Hence, there is room for further exploring the winter NAO-related SIC/BK and SCE/EUR anomalies.

The target diagnostics are the linear advection terms of T925 and q925: namely, the advection of climatological T925/q925 by the anomalous flow $[-v'.\ \nabla(\bar{T}, \bar{q})]$ and the advection of anomalous T925/q925 by the climatological flow $[-\ \bar{v}.\nabla(T', q')]$; the non-linear advection terms are negligible in terms of amplitude (not shown) (e.g., **?**). The advection of anomalous T925/q925 driven by the southwesterly climatological

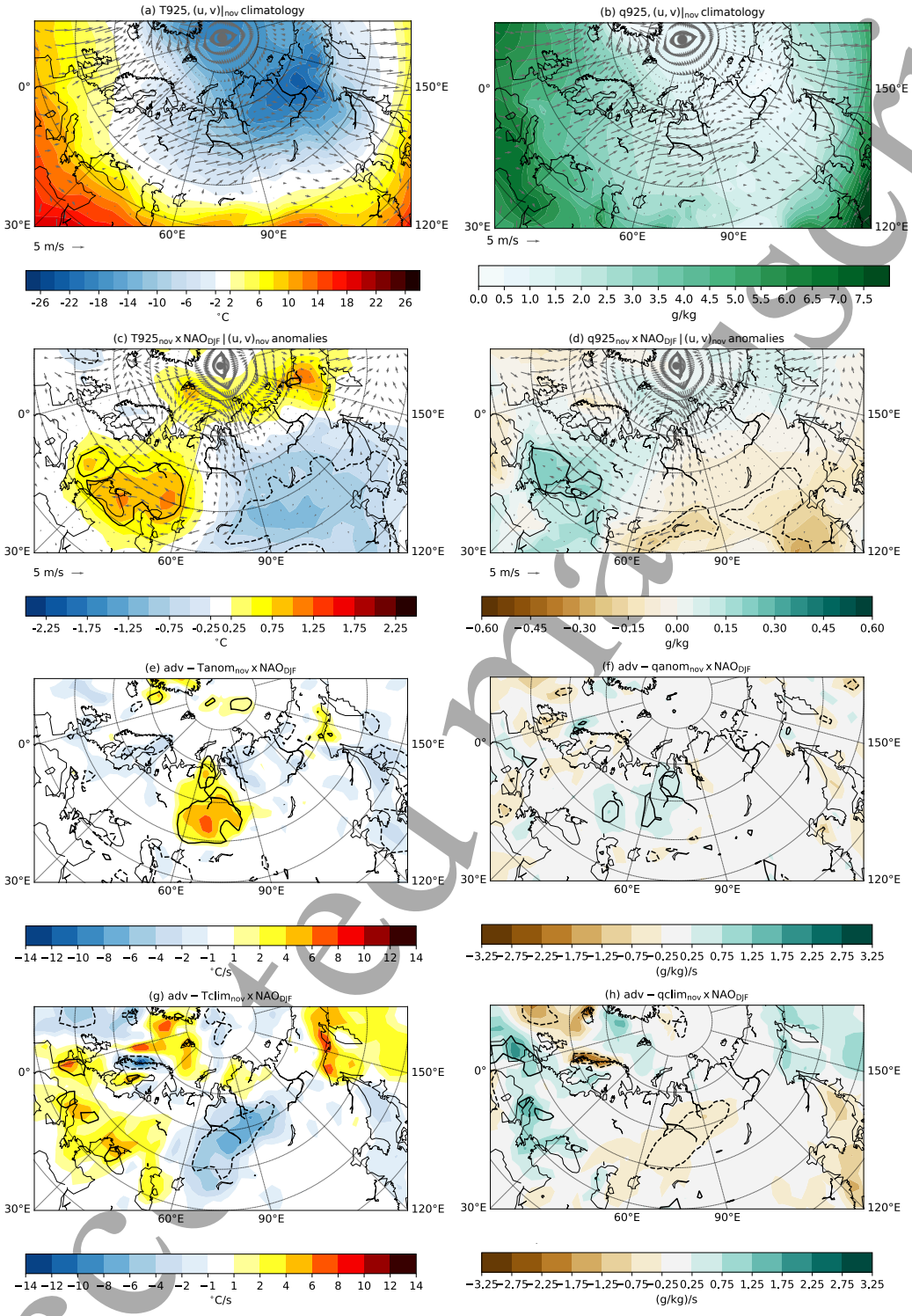

Figure 3. (a,b) Climatology of November air temperature (T925 ; °C) and specific humidity (q925 ; g/kg). Climatological wind at 925hPa ($\bar{u}, \bar{v}$; m/s) is overplotted with vectors. (c,d) Regression map of detrended T925 (°C) and q925 (g/kg) anomalies in November onto the winter NAO index-multiplied by -1. Anomalous wind at 925hPa (u',v'; m/s) is overplotted with vectors. (e,f) Regression map of the advection of anomalous T925 (°C/s) and q925 ((g/kg)/s) by the climatological flow in November onto the winter NAO index - multiplied by -1. (g,h) Regression map of the advection of climatological T925 (°C/s) and q925 ((g/kg)/s) by the anomalous flow in November onto the winter NAO index - multiplied by -1.

flow (Figure 3e,f), bringing warm and wet air masses from the Mediterranean, yield statistically significant anomalies upstream and over the Ural Mountains, i.e. windward. These warm and wet conditions do not contribute to the snow dipole preceding the NAO shown on Figure 1c. On the other hand, the advection of climatological T925/q925 by the anomalous flow yield statistically significant anomalies downstream (downwind) the Urals, namely over Siberia (Figure 3g,h). It implies that the wind anomalies preceding the NAO transport cold and dry air from the Arctic into Eurasia, indicative of land cooling and humidity sink associated with snowfall, particularly west of Baikal Lake (cf. Figures 1c,S3). This south-eastward transport, together with the induced warm and wet advection over the Mediterranean region (Figure 3g,h), suggests that the anomalous U-S anticyclone is the responsible of pushing the snow edge northward over western Eurasia and southward over eastern Eurasia, thereby generating the anomalous continental-scale dipole of snow cover (Figure 1c) and surface conditions(Figure 3c,d). These results contrast with previous works suggesting that increased SCE/EUR is a consequence of the moisture increase due to SIC/BK reduction (e.g., **?**, **?**), while our results suggest that the relationship is determined by the advection of climatological cold air from the Arctic, mediated by the anomalous atmospheric circulation.

3.4. Causality between SIC/BK, SCE/EUR and the U-S pattern

To gain insight on the causality between SIC/BK, SCE/EUR and the regional atmospheric circulation, turbulent (THF; sensible (SHF) plus latent (LHF)) and radiative (RHF; shortwave (SWR) plus longwave (LWR)) surface heat fluxes in November are analyzed (Figure 4).

Over the ocean, THF anomalies associated with the U-S pattern are dominated by downward heat flux, that is by ocean heat uptake, over the Norwegian Sea and the southern, ice-free Barents Sea (Figure 4a). These negative THF anomalies are likely

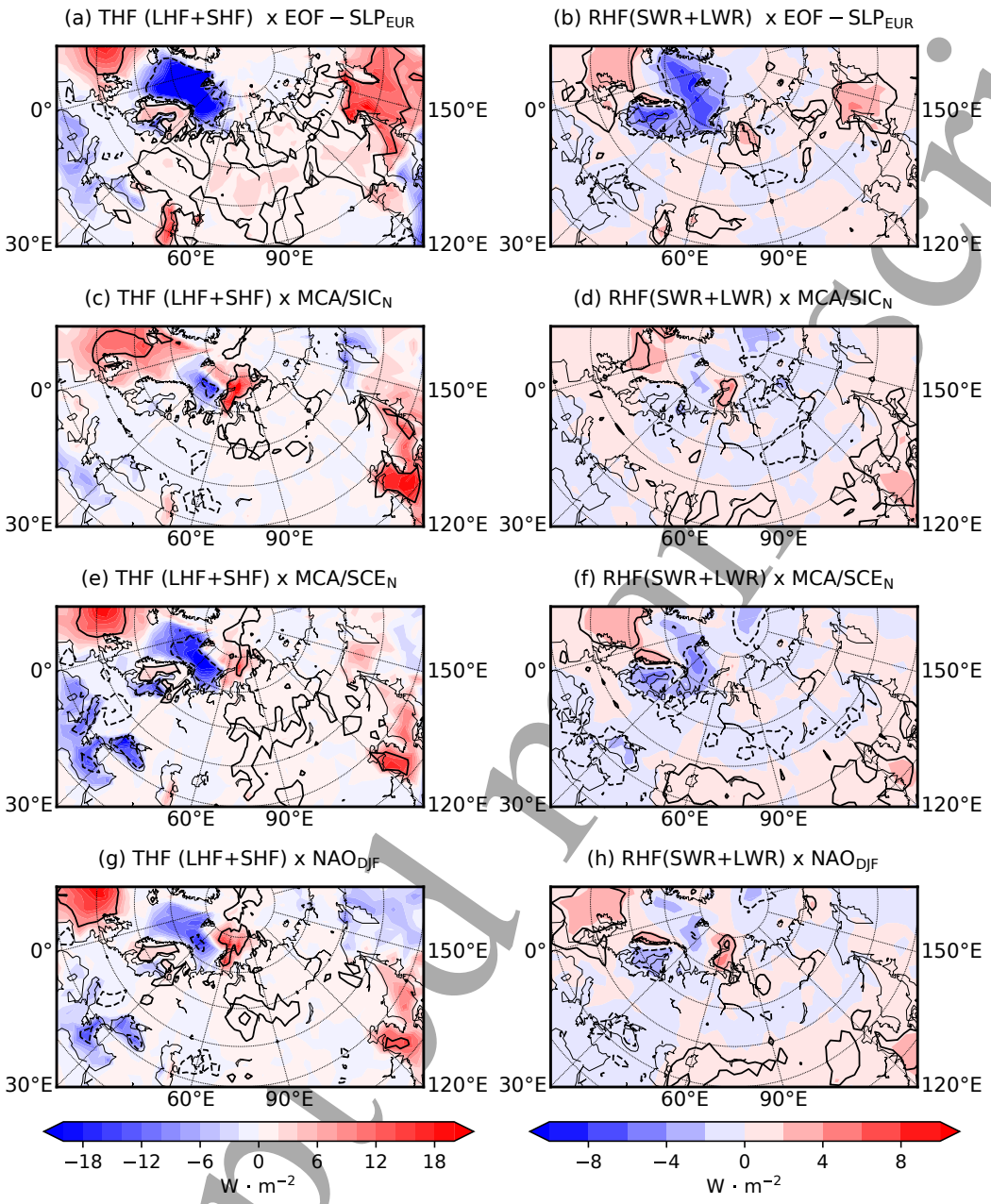

Figure 4. Regression map of detrended turbulent heat flux anomalies ($W \cdot m^{-2}$; a,c,e,g) and radiative heat flux anomalies ($W \cdot m^{-2}$; b,d,f,h) in November onto (a,b) the leading PC from the EOF analysis of November SLP over Eurasia (see Figure 2b), (c,d) the MCA/SIC$_N$ expansion coefficient, (e,f) the MCA/SCE$_N$ expansion coefficient and (g,h) the winter NAO index - multiplied by -1. Statistically significant areas at 95 % confidence level based on a two-tailed Student's test are contoured.

related to the southerly advection of warm and moist air induced by the anticyclonic circulation in the Siberian coast and the cyclonic circulation over the British Isles (Figure 2b); note that both SHF and LHF anomalies contribute almost equally (Figure S5). This anomalous THF pattern strongly resembles the atmosphere-driven THF EOF1 of **?**. And, consistently with this interpretation, the U-S/SCAND mode also shows negative RHF anomalies (Figure 4b), which are determined by increased downwelling LWR (Figure S6; e.g., **?**, and references therein). On the other hand, THF anomalies associated with MCA/SIC_N display enhanced upward heat flux over the Kara Sea and northern Barents Sea (Figure 4c). These positive THF anomalies, with contribution from both SHF and LHF (Figure S5), are related to sea-ice reduction and its retreat of the edge (Figure 1b). In this case, the anomalous THF pattern projects on the ice-driven THF EOF2 of **?**, associated with heat release over the newly-opened oceanic area (e.g., **?**). Note that this positive THF anomaly over BK is accompanied by a negative THF anomaly sharply south of the sea-ice edge (cf. Figures 1b,4c), which is the expected response to sea-ice reduction due to the modification of the air mass as it encounters open water (**?**, **?**, **?**, **?**), although in this framework we cannot discard a role from atmospheric advection as in Figure 4a. Consistent with the ice forcing of the atmosphere, note likewise that there is a positive RHF anomaly over BK (Figure 4d), controlled by emission of LWR (Figure S6). THF anomalies associated with MCA/SCE_N (Figure 4e) and the winter NAO (Figure 4g) show contributions from both signals, i.e. ocean heat uptake related to the U-S pattern (Figure 4a) and ocean heat release linked to SIC/BK (Figure 4c), with a larger and statistically significant influence of atmospheric advection/forcing over the Norwegian Sea for the former. It is worth stressing that both MCA/SCE_N and the winter NAO display positive THF anomalies over BK, which suggests that SIC/BK anomalies may contribute to tropospheric anomalies projecting

on U-S/SCAND-like variability (Figure 2). Several AGCM studies have reported U-S/SCAND circulation anomalies over Eurasia in response to SIC/BK reduction (e.g., **?**, **?**, **?**, **?**, **?**, **?**, **?**, **?**, **?**, **?**).

Over the continent, the snow-related THF anomalies depict statistically significant upward heat flux over central Eurasia, west of Baikal Lake, consistently among the regression maps onto the four time-series (Figure 4-left column). These positive THF anomalies are the result of the balance between snow melting and sublimation, with negative LHF anomalies (atmospheric cooling; Figure S5), and the heat transfer related to the advection of climatological cold air from the Arctic (Figure 3g) encountering a warmer surface, with positive SHF anomalies (atmospheric warming; Figure S5) that overcome the former. On the other hand, RHF anomalies systematically show downward heat flux over the same central Eurasian region, maybe weaker for the winter NAO (Figure 4-right column). In this case, the downwelling of LWR (atmospheric cooling) is stronger than the reflection of SWR (albedo effect leading to atmospheric warming; Figure S6). Note that over the snow-covered area south of Baikal Lake (Figures 1c, 2c-d) LWR and SWR anomalies are fully compensated (Figure S6). Finally, it is worth highlighting that over central Eurasia the net radiative cooling has to counteract the net turbulent warming (Figure 4), which may imply a low signal-to-noise atmospheric response to realistic snow anomalies.

4. Conclusions

According to previous observational studies (e.g., **?**, **?**, **?**), November SIC/BK represents the most robust "potential" predictor of the winter NAO based on eastern Arctic SIC variability. This work revealed that it corresponds to the leading EOF of SIC at regional and hemispheric scale, i.e. over the whole Arctic.

Concerning SCE/EUR, the leading covariability with winter SLP in the North Atlantic-European region is not statistically significant for October SCE, in contrast to previous observational studies using different approaches (e.g., **?**, **?**); while it is marginally significant for November SCE, in agreement with **?**. However, SCE/EUR does not display a dominant mode of variability in November which implies that it should not be considered as an "actual" predictor. It seems that the high correlation between November SCE/EUR and the winter NAO relies on the atmospheric precursor of the NAO itself, namely the Ural-Siberian anticyclone, in agreement with **?** and **?**.

Another aspect stressed in this study is that the Ural-Siberian anticyclone appears not to be associated with the Siberian High but with the regional, subpolar low-pressure system. The Ural-Siberian pattern stands for the third most prominent atmospheric pattern in the Northern Hemisphere after the PNA in the North Pacific and the NAO in the North Atlantic (e.g., **?**). Particularly in November, the Ural-Siberian anticyclone represents the leading EOF of SLP and is associated with the leading EOF of geopotential height at the upper troposphere (e.g., **?**, **?**); which corresponds to the SCAND pattern (e.g., **?**, **?**).

Finally, the variability of the Ural-Siberian pattern, which may include some SIC/BK forcing, appears to be responsible for the connection between the winter NAO and November SCE/EUR anomalies via advection of climatological temperature and humidity by the anomalous winds, transporting cold and dry air from the Arctic into Eurasia. The (potential) contribution of SCE/EUR to the Ural-Siberian pattern is questioned due to the competing effect of the associated radiative and turbulent heat flux anomalies over the snow-covered areas.

5. Acknowledgments

The research leading to these results has received funding from the European Commissions H2020 projects APPLICATE (GA 727862) and PRIMAVERA (GA 641727).JG-S was supported by the Ramón y Cajal programme (RYC-2016-21181). MM was supported by the MINECO project VOLCADEC (CGL201570177-R). JB has been supported by MINECO projects CGL2016-81828-REDT (AEI) and RTI2018-098693-B643-C32 (AEI). The authors thank Hervé Douville (CNRM/Météo-France) and Guillaume Gastineau (LOCEAN/IPSL, France) for useful discussions.

6. Data availability statement

The data that support the findings of this study are openly available.

- Sea Ice data HadISST (Hadley Center Sea Ice and Sea Surface Temperature (DOI:10.1029/2002JD002670)
- Snow Cover data from the Global Snow Laboratory at Rutgers University (DOI: 10.7289/V5N014G9)
- Atmospheric variables data from ERA-Interim reanalysis available from the European Center for Medium-Range Weather Forecasts (ECMWF)(DOI:10.1002/qj.828).

7. References

[1] Hurrell JW, Kushnir Y, Ottersen G, Visbeck M. An overview of the North Atlantic oscillation. The North Atlantic Oscillation: climatic significance and environmental impact. 2003;134:1–35.

[2] Hurrell JW, Deser C. North Atlantic climate variability: the role of the North Atlantic Oscillation. Journal of Marine Systems. 2010;79(3-4):231–244.

[3] Cohen J, Jones J. A new index for more accurate winter predictions. Geophysical Research Letters. 2011;38(21).

[4] Scaife A, Arribas A, Blockley E, Brookshaw A, Clark R, Dunstone N, et al. Skillful long-range prediction of European and North American winters. Geophysical Research Letters. 2014;41(7):2514–2519.

[5] García-Serrano J, Frankignoul C, Gastineau G, De La Càmara A. On the predictability of the winter Euro-Atlantic climate: lagged influence of autumn Arctic sea ice. Journal of Climate. 2015;28(13):5195–5216.

[6] Dunstone N, Smith D, Scaife A, Hermanson L, Eade R, Robinson N, et al. Skilful predictions of the winter North Atlantic Oscillation one year ahead. Nature Geoscience. 2016;9(11):809.

[7] Wang L, Ting M, Kushner P. A robust empirical seasonal prediction of winter NAO and surface climate. Scientific reports. 2017;7(1):279.

[8] King MP, Hell M, Keenlyside N. Investigation of the atmospheric mechanisms related to the autumn sea ice and winter circulation link in the Northern Hemisphere. Climate dynamics. 2016;46(3-4):1185–1195.

[9] Kim BM, Son SW, Min SK, Jeong JH, Kim SJ, Zhang X, et al. Weakening of the stratospheric polar vortex by Arctic sea-ice loss. Nature communications. 2014;5:ncomms5646.

[10] Nakamura T, Yamazaki K, Iwamoto K, Honda M, Miyoshi Y, Ogawa Y, et al. A negative phase shift of the winter AO/NAO due to the recent Arctic sea-ice reduction in late autumn. Journal of Geophysical Research: Atmospheres. 2015;120(8):3209–3227.

[11] Nakamura T, Yamazaki K, Iwamoto K, Honda M, Miyoshi Y, Ogawa Y, et al. The stratospheric pathway for Arctic impacts on midlatitude climate. Geophysical Research Letters. 2016;43(7):3494–3501.

[12] Sun L, Deser C, Tomas RA. Mechanisms of stratospheric and tropospheric circulation response to projected Arctic sea ice loss. Journal of Climate. 2015;28(19):7824–7845.

[13] Kug JS, Jeong JH, Jang YS, Kim BM, Folland CK, Min SK, et al. Two distinct influences of Arctic warming on cold winters over North America and East Asia. Nature Geoscience. 2015;8(10):759.

[14] García-Serrano J, Frankignoul C, King M, Arribas A, Gao Y, Guemas V, et al. Multi-model assessment of linkages between eastern Arctic sea-ice variability and the Euro-Atlantic atmospheric circulation in current climate. Climate Dynamics. 2017;49(7-8):2407–2429.

[15] Cohen J, Screen JA, Furtado JC, Barlow M, Whittleston D, Coumou D, et al. Recent Arctic amplification and extreme mid-latitude weather. Nature geoscience. 2014;7(9):627–637.

[16] Kidston J, Scaife AA, Hardiman SC, Mitchell DM, Butchart N, Baldwin MP, et al. Stratospheric

influence on tropospheric jet streams, storm tracks and surface weather. Nature Geoscience. 2015;8(6):433.

[17] Screen JA, Deser C, Smith DM, Zhang X, Blackport R, Kushner PJ, et al. Consistency and discrepancy in the atmospheric response to Arctic sea-ice loss across climate models. Nature Geoscience. 2018;11(3):155–163.

[18] Peings Y. Ural Blocking as a Driver of Early-Winter Stratospheric Warmings. Geophysical Research Letters. 2019;46(10):5460–5468.

[19] Blackport R, Screen JA, van der Wiel K, Bintanja R. Minimal influence of reduced Arctic sea ice on coincident cold winters in mid-latitudes. Nature Climate Change. 2019;9(9):697–704.

[20] Cohen J, Rind D. The effect of snow cover on the climate. Journal of Climate. 1991;4(7):689–706.

[21] Cohen J, Barlow M, Kushner PJ, Saito K. Stratosphere–troposphere coupling and links with Eurasian land surface variability. Journal of Climate. 2007;20(21):5335–5343.

[22] Gong G, Entekhabi D, Cohen J. Modeled Northern Hemisphere winter climate response to realistic Siberian snow anomalies. Journal of Climate. 2003;16(23):3917–3931.

[23] Gong G, Entekhabi D, Cohen J. Relative impacts of Siberian and North American snow anomalies on the winter Arctic Oscillation. Geophysical Research Letters. 2003;30(16).

[24] Gong G, Entekhabi D, Cohen J. Orographic constraints on a modeled Siberian snow–tropospheric–stratospheric teleconnection pathway. Journal of Climate. 2004;17(6):1176–1189.

[25] Fletcher CG, Kushner PJ, Cohen J. Stratospheric control of the extratropical circulation response to surface forcing. Geophysical Research Letters. 2007;34(21).

[26] Fletcher CG, Hardiman SC, Kushner PJ, Cohen J. The dynamical response to snow cover perturbations in a large ensemble of atmospheric GCM integrations. Journal of Climate. 2009;22(5):1208–1222.

[27] Peings Y, Saint-Martin D, Douville H. A numerical sensitivity study of the influence of Siberian snow on the northern annular mode. Journal of Climate. 2012;25(2):592–607.

[28] Orsolini Y, Senan R, Vitart F, Balsamo G, Weisheimer A, Doblas-Reyes F. Influence of the Eurasian snow on the negative North Atlantic Oscillation in subseasonal forecasts of the cold winter 2009/2010. Climate Dynamics. 2016;47(3-4):1325–1334.

[29] Henderson GR, Peings Y, Furtado JC, Kushner PJ. Snow–atmosphere coupling in the Northern Hemisphere. Nature Climate Change. 2018;8(11):954–963.

[30] Kolstad E, Screen J. Nonstationary relationship between autumn Arctic sea ice and the winter

North Atlantic oscillation. Geophysical Research Letters. 2019;46(13):7583–7591.

[31] Siew PYF, Li C, Sobolowski SP, King MP. Intermittency of Arctic-midlatitude teleconnections: stratospheric pathway between autumn sea ice and the winter NAO. Weather and Climate Dynamics Discussions. 2019;2019:1–23.

[32] Peings Y, Brun E, Mauvais V, Douville H. How stationary is the relationship between Siberian snow and Arctic Oscillation over the 20th century? Geophysical Research Letters. 2013;40(1):183–188.

[33] Douville H, Peings Y, Saint-Martin D. Snow-(N) AO relationship revisited over the whole twentieth century. Geophysical Research Letters. 2017;44(1):569–577.

[34] Deser C, Tomas R, Alexander M, Lawrence D. The seasonal atmospheric response to projected Arctic sea ice loss in the late twenty-first century. Journal of Climate. 2010;23(2):333–351.

[35] Cohen JL, Furtado JC, Barlow MA, Alexeev VA, Cherry JE. Arctic warming, increasing snow cover and widespread boreal winter cooling. Environmental Research Letters. 2012;7(1):014007.

[36] Cohen J, Jones J, FurtadO JC, Tziperman E. Warm Arctic, cold continents: A common pattern related to Arctic sea ice melt, snow advance, and extreme winter weather. Oceanography. 2013;26(4):150–160.

[37] Ghatak D, Deser C, Frei A, Gong G, Phillips A, Robinson DA, et al. Simulated Siberian snow cover response to observed Arctic sea ice loss, 1979–2008. Journal of Geophysical Research: Atmospheres. 2012;117(D23).

[38] Liu J, Curry JA, Wang H, Song M, Horton RM. Impact of declining Arctic sea ice on winter snowfall. Proceedings of the National Academy of Sciences. 2012;.

[39] Li F, Wang H. Autumn sea ice cover, winter Northern Hemisphere annular mode, and winter precipitation in Eurasia. Journal of Climate. 2012;26(11):3968–3981.

[40] Wegmann M, Orsolini Y, Vázquez M, Gimeno L, Nieto R, Bulygina O, et al. Arctic moisture source for Eurasian snow cover variations in autumn. Environmental Research Letters. 2015;10(5):054015.

[41] Gastineau G, García-Serrano J, Frankignoul C. The influence of autumnal Eurasian snow cover on climate and its link with Arctic sea ice cover. Journal of Climate. 2017;30(19):7599–7619.

[42] Smith DM, Screen JA, Deser C, Cohen J, Fyfe JC, García-Serrano J, et al. The Polar Amplification Model Intercomparison Project (PAMIP) contribution to CMIP6: investigating the causes and consequences of polar amplification. Geoscientific Model Development. 2019;12:1139–1164.

[43] von Storch H, Zwiers FW. Statistical Analysis in Climate Research. 1st ed. Cambridge: Cambridge University Press; 1999.

[44] Bretherton CS, Smith C, Wallace JM. An intercomparison of methods for finding coupled patterns in climate data. Journal of climate. 1992;5(6):541–560.

[45] Rayner N, Parker DE, Horton E, Folland C, Alexander L, Rowell D, et al. Global analyses of sea surface temperature, sea ice, and night marine air temperature since the late nineteenth century. Journal of Geophysical Research: Atmospheres. 2003;108(D14).

[46] Robinson DA, Dewey KF, Heim Jr RR. Global snow cover monitoring: An update. Bulletin of the American Meteorological Society. 1993;74(9):1689–1696.

[47] Dee DP, Uppala SM, Simmons A, Berrisford P, Poli P, Kobayashi S, et al. The ERA-Interim reanalysis: Configuration and performance of the data assimilation system. Quarterly Journal of the royal meteorological society. 2011;137(656):553–597.

[48] Koenigk T, Caian M, Nikulin G, Schimanke S. Regional Arctic sea ice variations as predictor for winter climate conditions. Climate Dynamics. 2016;46(1-2):317–337.

[49] King MP, García-Serrano J. Potential ocean–atmosphere preconditioning of late autumn Barents-Kara sea ice concentration anomaly. Tellus A: Dynamic Meteorology and Oceanography. 2016;68(1):28580.

[50] Sorokina SA, Li C, Wettstein JJ, Kvamstø NG. Observed atmospheric coupling between Barents Sea ice and the warm-Arctic cold-Siberian anomaly pattern. Journal of Climate. 2016;29(2):495–511.

[51] Yang XY, Yuan X, Ting M. Dynamical link between the Barents–Kara sea ice and the Arctic Oscillation. Journal of Climate. 2016;29(14):5103–5122.

[52] Han S, Sun J. Impacts of autumnal Eurasian snow cover on predominant modes of boreal winter surface air temperature over Eurasia. Journal of Geophysical Research: Atmospheres. 2018;123(18):10–076.

[53] Cohen J, Saito K, Entekhabi D. The role of the Siberian high in Northern Hemisphere climate variability. Geophysical Research Letters. 2001;28(2):299–302.

[54] Cohen J, Salstein D, Saito K. A dynamical framework to understand and predict the major Northern Hemisphere mode. Geophysical Research Letters. 2002;29(10):51–1.

[55] North GR, Bell TL, Cahalan RF, Moeng FJ. Sampling errors in the estimation of empirical orthogonal functions. Monthly weather review. 1982;110(7):699–706.

[56] Smoliak BV, Wallace JM. On the leading patterns of Northern Hemisphere sea level pressure variability. Journal of the Atmospheric Sciences. 2015;72(9):3469–3486.

[57] Mori M, Watanabe M, Shiogama H, Inoue J, Kimoto M. Robust Arctic sea-ice influence on the frequent Eurasian cold winters in past decades. Nature Geoscience. 2014;7(12):869.

[58] Tyrlis E, Manzini E, Bader J, Ukita J, Hisahi N, Matei D. Ural blocking driving extreme Arctic sea-ice loss, cold eurasia and stratospheric vortex weakening in autumn and early winter 2016-2017. Journal of Geophysical Research: Atmospheres. 2019;124:11313–11329.

[59] King MP, Herceg-Bulić I, Kucharski F, Keenlyside N. Interannual tropical Pacific sea surface temperature anomalies teleconnection to Northern Hemisphere atmosphere in November. Climate dynamics. 2018;50(5-6):1881–1899.

[60] Bueh C, Nakamura H. Scandinavian pattern and its climatic impact. Quarterly Journal of the Royal Meteorological Society: A journal of the atmospheric sciences, applied meteorology and physical oceanography. 2007;133(629):2117–2131.

[61] Liu Y, Wang L, Zhou W, Chen W. Three Eurasian teleconnection patterns: Spatial structures, temporal variability, and associated winter climate anomalies. Climate dynamics. 2014;42(11-12):2817–2839.

[62] Kuroda Y, Kodera K. Role of planetary waves in the stratosphere-troposphere coupled variability in the northern hemisphere winter. Geophysical Research Letters. 1999;26(15):2375–2378.

[63] Takaya K, Nakamura H. Precursory changes in planetary wave activity for midwinter surface pressure anomalies over the Arctic. Journal of the Meteorological Society of Japan Ser II. 2008;86(3):415–427.

[64] Orsolini YJ, Kindem I, Kvamstø N. On the potential impact of the stratosphere upon seasonal dynamical hindcasts of the North Atlantic Oscillation: a pilot study. Climate dynamics. 2011;36(3-4):579–588.

[65] Cohen J, Furtado JC, Jones J, Barlow M, Whittleston D, Entekhabi D. Linking Siberian snow cover to precursors of stratospheric variability. Journal of Climate. 2014;27(14):5422–5432.

[66] Cohen J, Foster J, Barlow M, Saito K, Jones J. Winter 2009–2010: A case study of an extreme Arctic Oscillation event. Geophysical Research Letters. 2010;37(17).

[67] Vallis GK, Gerber EP. Local and hemispheric dynamics of the North Atlantic Oscillation, annular patterns and the zonal index. Dynamics of atmospheres and oceans. 2008;44(3-4):184–212.

[68] Inoue J, Hori ME, Takaya K. The role of Barents Sea ice in the wintertime cyclone track and

emergence of a warm-Arctic cold-Siberian anomaly. Journal of Climate. 2012;25(7):2561–2568.

[69] Orsolini YJ, Kvamstø NG. Role of Eurasian snow cover in wintertime circulation: Decadal simulations forced with satellite observations. Journal of Geophysical Research: Atmospheres. 2009;114(D19).

[70] Allen R, Zender C. Effects of continental-scale snow albedo anomalies on the wintertime Arctic oscillation. Journal of Geophysical Research: Atmospheres. 2010;115(D23).

[71] Honda M, Inoue J, Yamane S. Influence of low Arctic sea-ice minima on anomalously cold Eurasian winters. Geophysical Research Letters. 2009;36(8).

[72] Orsolini YJ, Senan R, Benestad RE, Melsom A. Autumn atmospheric response to the 2007 low Arctic sea ice extent in coupled ocean–atmosphere hindcasts. Climate dynamics. 2012;38(11-12):2437–2448.

[73] Wallace JM, Hobbs PV. Atmospheric science: an introductory survey. vol. 92. Elsevier; 2006.

[74] Magnusdottir G, Deser C, Saravanan R. The effects of North Atlantic SST and sea ice anomalies on the winter circulation in CCM3. Part I: Main features and storm track characteristics of the response. Journal of Climate. 2004;17(5):857–876.

[75] Deser C, Magnusdottir G, Saravanan R, Phillips A. The effects of North Atlantic SST and sea ice anomalies on the winter circulation in CCM3. Part II: Direct and indirect components of the response. Journal of Climate. 2004;17(5):877–889.

[76] Deser C, Tomas RA, Peng S. The transient atmospheric circulation response to North Atlantic SST and sea ice anomalies. Journal of Climate. 2007;20(18):4751–4767.

[77] Grassi B, Redaelli G, Visconti G. Arctic sea ice reduction and extreme climate events over the Mediterranean region. Journal of Climate. 2013;26(24):10101–10110.

[78] McCusker KE, Fyfe JC, Sigmond M. Twenty-five winters of unexpected Eurasian cooling unlikely due to Arctic sea-ice loss. Nature Geoscience. 2016;9(11):838.

[79] Ruggieri P, Kucharski F, Buizza R, Ambaum M. The transient atmospheric response to a reduction of sea-ice cover in the Barents and Kara Seas. Quarterly Journal of the Royal Meteorological Society. 2017;143(704):1632–1640.

[80] Furtado J, Cohen J, Tziperman E. The combined influences of autumnal snow and sea ice on Northern Hemisphere winters. Geophysical Research Letters. 2016;43(7):3478–3485.